Measurement of the Spin Relaxation Time of Single Electrons in a Silicon Metal-Oxide-Semiconductor-Based Quantum Dot

M. Xiao,* M. G. House, and H. W. Jiang

Department of Physics and Astronomy, University of California at Los Angeles,
405 Hilgard Avenue, Los Angeles, California 90095, USA
(Received 1 October 2009; published 2 March 2010)

We demonstrate direct detection of individual electron spin states, together with measurement of spin relaxation time (T_1), in silicon metal-oxide-semiconductor-based quantum dots (QD). Excited state spectroscopy of the QD has been performed using a charge-sensing technique. T_1 of single spin excited states has been done in the time domain by a pump-and-probe method. For an odd and an even number of electrons, we found a magnetic field dependent and invariant T_1, respectively.

The potential of using individual electron spin states in a semiconductor quantum dot for quantum information processing has triggered a stream of experimental investigations in recent years to detect and manipulate single spins in the few-electron limit [1]. The spin relaxation time T_1, an important measure of the interaction between a two-level quantum system and its environment, has now been successfully measured in GaAs based quantum dots and in self-assembled InGaAs quantum dots for spin-flip transitions between two magnetic field induced Zeeman sublevels [2–4], and between a singlet ground state and a triplet excited state [5–7]. The distinct band structure makes Si differ from GaAs in a number of ways, which are important to the spin relaxation process, such as the nature of the electron-phonon coupling [1,8–12], the strength of spin-orbital interaction, the closely spaced levels due to the valley degeneracy [13], and a vanishingly small hyperfine interaction with nuclear spins as there is only 5% silicon isotope with nonzero nuclear spins. Therefore the dominating mechanism leading to spin relaxation in a Si quantum dots (QDs) needs to be experimentally explored.

However, comparable electrostatically defined Si devices, which have only started to emerge very recently [14], usually do not have the stability and/or controllability required for the demanding spin relaxation measurements. Here we present such a T_1 measurement of individual electron spins in the few-electron regime of a Si MOS-based quantum dot. Excellent stability and controllability of the devices were achieved through continuous technology improvements. These allow us to directly study the spin state spectroscopy of individual electrons. T_1 was subsequently measured using pump-and-probe technique.

The device fabrication started with a commercial Si/SiO_2 wafer with a 50 nm thick thermal oxide. First, multiple confinement gates were fabricated by electron-beam-lithography. Then, a 100 nm Al_2O_3 layer was grown epitaxially by atomic layer deposition. Finally, a global gate was fabricated to accumulate 2D electron gas (2DEG) near the interface of the Si and SiO_2 across the entire

sample. The 2DEG mobility (with confinement gates inactive) reaches 2×10^4 $cm^2/V\,s$ when electron density is in the working range of $1-3 \times 10^{11}$ cm^{-2}. Figure 1 shows the pattern of the confinement gates and the cross-sectional view of the device. Architecturally, this double insulating layered Si MOS-based quantum dot structure is similar to those reported in a number of earlier publications [14].

With the top global gate voltage set at a fixed positive value, lower voltages are applied to the six confinement gates LT, RT, LB, RB, P, and Q to shape the QD and the charge-sensing channel. While gate P was used primarily to control the number of electrons in the QD, gates LT-LB and RT-RB controlled the transparency of the left and right barriers, respectively. Gate Q, along with RT and LT, formed a 1D charge-sensing channel to count the number of electrons via capacitive coupling. A small gap between LT and RT was created to maximize this capacitive coupling without passing through direct electron tunneling. A dc biasing voltage of 0.8 mV was applied across the sens-
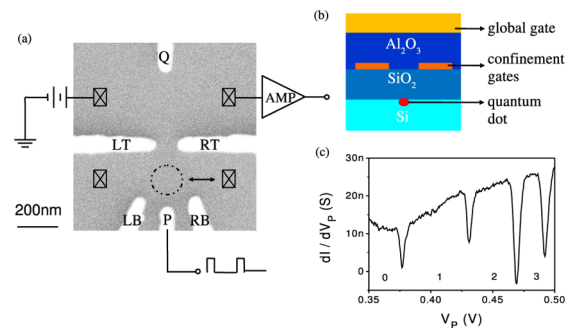
FIG. 1 (color online).   (a) Scanning electron micrograph of the confinement gates that define the QD (open circle), along with the measurement setup. (b) The cross-sectional view of the device. (c) A typical trace of the differential conductance signal of the charge-sensing channel as a function of the dc bias V_P, $V_{LT} = -0.1$ V, $V_{RT} = -0.16$ V, $V_{LB} = -0.85$ V, $V_{RB} = -0.44$ V, $V_Q = -0.7$ V, and $V_{global} = 3.2$ V. A square pulse of $\Delta V_P = 3$ mV and $f = 10$ kHz was superimposed to dc bias on gate P to dynamically charge and discharge the QD.

ing channel while the resulting current was amplified by a high-bandwidth (200 kHz) and low-noise (130 fA/$\sqrt{\text{Hz}}$) current amplifier (FEMTO DLPCA-200) at a gain of 10^8 V/A. The resistance of the sensing channel was set by gate Q to about 10^5 ohms, which corresponds to a bandwidth of 50 kHz. Also, a Stanford Research System SRS535 Pulse/Delay Digital Generator was used to provide the electrical pulses and a SRS 830 lock-in amplifier was used to record time integrated signal. An Agilent Infiniium 54855A oscilloscope with a sampling rate up to 5 G/S was used for the time-resolved measurements. The experiments were done in an Oxford top-loading He3 refrigerator with a base temperature of 300 mK. A magnetic field was applied along the plane of the device.

We can detect the addition of an electron to the QD by tracking changes in the 1D channel current. Typically the addition of a single electron would result in a reduction in the total current of about 1%. To offset the large current background, we used a lock-in detection method developed earlier for GaAs work [15]. A square shaped pulse was superimposed on the dc bias on P. A lock-in detector in sync with the pulse frequency measured the change of the channel current due to the pulse modulation. Figure 1(c) shows a typical trace of the lock-in signal as a function of the voltage applied to gate P. The four dips indicate the transitions in the charge states by addition or subtraction of single electrons. The QD was put into an environment in which the left barrier was essentially opaque and the tunneling frequency between the right barrier and the reservoir was about 1 kHz. The tunneling rate can be tuned continuously from 100 Hz to 30 kHz for the last few electrons and can be measured in time domain by an oscilloscope. The four dips shown are most likely the last four electrons in the QD, as we could not detect any additional dips as the QD was further squeezed. We verified that the absence of the additional peak was not due to the closure of the QD by increasing the voltages on RT and RB (i.e., the transparency of the right barrier).

The information contained in the signal goes beyond simple charge counting. For instance, varying the pulse amplitude can reveal excited states. Figures 2(a) and 2(b) show in a gray scale plot the derivative of the signal as a function of the pulse amplitude and gate voltage for the $N = 0 \leftrightarrow N = 1$ and the $N = 1 \leftrightarrow N = 2$ transitions, respectively. In each case, a triangular pattern with an extra interior line (indicated by the arrow) can be visualized. The left line is due to the front edge of the pulse beginning the process of electron loading while the right line is for the point where the ground-state electron is unloading. An extra interior line [dark for Fig. 2(a) and bright for Fig. 2(b)] indicates an excited state. The excited state becomes visible when the excitation frequency is high enough in comparison to the relaxation rate from the excited state to the ground state. As shown in the Fig. 2(d), a pulse with sufficiently high amplitude can populate either the ground state or the excited state during
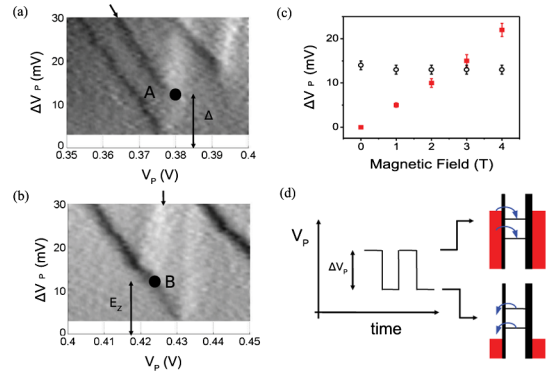
FIG. 2 (color online).   Gray scale plots of the derivative of the current signal with respect to ΔV_p as a function of ΔV_p and V_p at $B = 3$ T for (a) the $N = 0$ to $N = 1$ transition (open circles), and (b) the $N = 1$ to $N = 2$ transition (closed squares). (c) Pulse amplitude for the termination points of the excited state line, a measure of the QD level spacing and the Zeeman splitting, as a function of the magnetic field. (d) Schematic electrochemical potential diagrams illustrate the charging and discharging of the QD during the high and low voltages of the pulse.

the high-voltage cycle and depopulate during the low-voltage cycle. We found that the interior line terminates on the right side for the 0–1 transition and terminates on the left side for the 1–2 transition. Following arguments from excited state spectroscopy (see Fig. 5 of Ref. [1]), both point A and B measure the energy difference between one of the excited states of $N = 1$ and the ground state of $N = 1$.

We studied the dependence of the termination points on a magnetic field applied parallel to the Si/SiO$_2$ interface and found that point A was largely independent of the magnetic field while the termination point B varied linearly with the field, as shown in Fig. 2(c). For this reason, point B is most likely a measure of the spacing of the two Zeeman sublevels for $N = 1$ electron, and point A is assigned to the orbital level spacing of the QD. Assuming the g factor of an electron in Si to be 2, a conversion factor between the pulse voltage and the energy can be extracted from the magnetic field dependence of the energy level spacing to be 27 meV/V. This conversion factor is consistent with that obtained from the transport measurement of the Coulomb diamonds. The B-independent energy spacing is therefore about 0.4 meV. The Coulomb charging energies needed to add an additional electron to $N = 1$, $N = 2$, and $N = 3$ QD are 5 meV, 3.8 meV, and 3 meV, respectively.

Having established the energies of the QD charge states, we now present a relaxation measurement for both the $N = 1$ and $N = 2$ QD. For the $N = 1$ QD, it should be a spin-flip transition between two magnetic field induced Zeeman sublevels, as discussed for point B. We used a two-step pulse sequence, adapted again from earlier work on GaAs QDs [2,4,6]. Figure 3 illustrates schematically the working principle of this electrical pump-and-probe technique. The QD during the first phase is emptied or initialized as
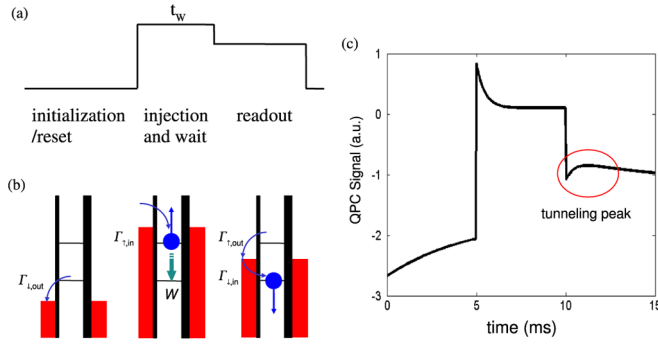
FIG. 3 (color online).   (a) Two-step pulse sequence used for the T_1 measurement, (b) Schematic electrochemical potential diagrams for the three stages of the pulse. (c) Simulated current signal in time domain, averaged over many cycles of such a pulse sequence. The simulation parameters used were $\Gamma_{\uparrow,\text{in}} = \Gamma_{\uparrow,\text{out}} = 2$ kHz, $\Gamma_{\downarrow,\text{in}} = \Gamma_{\downarrow,\text{out}} = 0.2$ kHz, $W = 100$ Hz.

the Fermi level sits below the ground state. The Fermi level is then moved above both the down-spin ground and the up-spin excited states during the second phase. After waiting for a certain period of time t_W, the Fermi level is placed to the middle of the two levels for the state readout during third phase. For $t_W \gg T_1$, the electron is expected to relax to the ground state and there should be no tunneling from the QD to the reservoir. However, for short t_W, if the electron still remains in the excited state, the

electron tunnels out and subsequently tunnels back into the ground state, generating a transient signal in the charge-sensing channel. In principle, this tunneling event can be detected by applying a single pulse (i.e., single-shot measurement) [2,4]. However, the relatively poor signal-to-noise ratio of our detection, about 1:5, prevented us from seeing the tunneling event in real time. We therefore applied multiple pulses and averaged the channel signal over several thousand times. The resulting signal was captured by a digital oscilloscope. Displayed in Fig. 4(a), typical traces in the readout phase show a broadened peak. The broadening is expected from the statistical distributions of the tunneling electron in and out of the QD as simulated in Fig. 3(c).

For the simulation, we have developed a rate equation model to determine the expectation value of the number of electrons on the quantum dot, which is proportional to the averaged signal over many periods of the pulse sequence. The probabilities that the quantum dot is in each of the three allowed states (electron spin-up, spin-down, and no electron) are contained in the vector $\mathbf{p} = (p_\uparrow, p_\downarrow, p_0)$, which evolves in time according to the equation: $d\mathbf{p}/dt = \mathbf{Q}\mathbf{p}$. Here $\mathbf{Q}$ is a transition matrix that describes the instantaneous transition rates between the states. There are three matrices corresponding to the initialization or reset, injection and wait, and readout phases of the cycle, respectively:

$$\mathbf{Q}_1 = \begin{pmatrix} -W - \Gamma_{\uparrow,\text{out}} & 0 & 0 \\ W & -\Gamma_{\downarrow,\text{out}} & 0 \\ \Gamma_{\uparrow,\text{out}} & \Gamma_{\downarrow,\text{out}} & 0 \end{pmatrix} \quad \mathbf{Q}_2 = \begin{pmatrix} -W & 0 & \Gamma_{\uparrow,\text{in}} \\ W & 0 & \Gamma_{\downarrow,\text{in}} \\ 0 & 0 & -\Gamma_{\downarrow,\text{in}} - \Gamma_{\uparrow,\text{in}} \end{pmatrix} \quad \mathbf{Q}_3 = \begin{pmatrix} -W - \Gamma_{\uparrow,\text{out}} & 0 & 0 \\ W & 0 & \Gamma_{\downarrow,\text{in}} \\ \Gamma_{\uparrow,\text{out}} & 0 & -\Gamma_{\downarrow,\text{in}} \end{pmatrix},$$

where $\Gamma_{\uparrow(\downarrow),\text{in(out)}}$ is the tunneling rate into (out of) the $|\uparrow\rangle (|\downarrow\rangle)$ state, and W is the rate of relaxation from $|\uparrow\rangle$ to $|\downarrow\rangle$. We are most interested in the probability vector during the readout phase:

$$\mathbf{p}(t) = e^{\mathbf{Q}_3(t - t_2 - t_1)} e^{\mathbf{Q}_2 t_2} e^{\mathbf{Q}_1 t_1} \mathbf{p}(0), \qquad t_2 \leq t \leq t_2 + t_3,$$

where t_1, t_2, and t_3 are the pulse width for each of the three phases, respectively. t_2 is just equivalent to the waiting time t_W. $\mathbf{p}(0) = (0, 0, 1)$, suppose the electron is always emptied out in the initialization phase. The channel current $I(t)$ is proportional to $p_\uparrow(t) + p_\downarrow(t)$, which during the readout phase first increases approximately like $e^{\Gamma_{\uparrow,\text{out}}(t - t_2)}$, as spin-up electrons tunnel out of the quantum dot, and then decreases approximately like $e^{-\Gamma_{\downarrow,\text{in}}(t - t_2)}$, as spin-down electrons tunnel back in. This is labeled as the "tunneling peak" in Fig. 3(c). This signals the occupation of the spin-up state and its amplitude decreases as we increase t_2 because spin-up electrons relax to spin-down. In the limit that the tunneling rates are much faster than W, the dependence on t_2 is e^{-Wt_2}, in which case we can determine the relaxation rate W by fitting the tunneling peak amplitude as a function of t_2 to an exponential decay curve. When W is on the same order of magnitude as the tunneling rates, as it

sometimes is in our experiment, the rate equation model is useful for comparing to the observed data.

In Fig. 4(a) the tunneling peak is shown for several waiting times at $B = 4$ T. The trend of the reduction of the height with increasing waiting time can be clearly seen. This dependence is plotted in Fig. 4(b) and was fit to an exponential decay $A = e^{-t_W/T_1}$ to extract T_1. Our measurement capability is limited by the charge detector bandwidth at the short-time scales. The relaxation rates from the excited state to ground state are plotted as a function of the magnetic field. For the $N = 1$ QD the relaxation rate shows a strong dependence on B. In contrast, the relaxation time is essentially a constant of around 5 ms for the $N = 2$ QD.

For a $N = 1$ QD, in the presence of a magnetic field, the main mechanism for electrons to relax from one Zeeman split sublevel to another is through the stochastic electric-field fluctuations caused by phonons of the host materials [1,8–12]. The coupling between the magnetic fields of spins to the electrical fields of phonons can be facilitated by the relatively strong spin-orbital coupling (SOC) in semiconductors. For GaAs QDs, it has been demonstrated that the spin relaxation rate T_1^{-1} depends both on the piezoelectric effect (i.e., piezoelectric phonons) and the
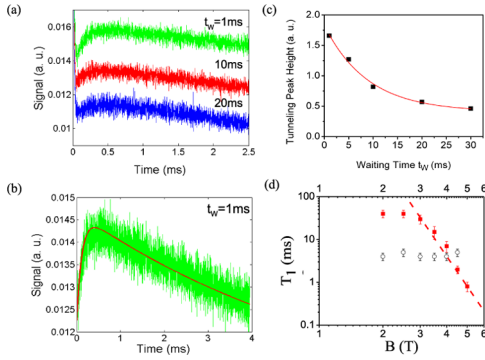
FIG. 4 (color online).   (a) The tunneling signal at the readout phase is displayed for three different waiting times. A vertical offset is applied to the curves for visual clarity. (b) An example of fit to the model for the $t_W = 1$ ms data. (c) The amplitude of the tunneling signal, proportional to the probability of occupying the spin-up state, as a function of t_W. The amplitude is fitted to an exponential curve that gives $T_1 \approx 10$ ms. (c) The relaxation times for the $N = 1$ (closed squares) and $N = 2$ (open dots) as a function of the magnetic field. The dashed line projects a B^7 dependence.

spatial deformation of the crystal structure (i.e., deformation potential phonons) [1,2,4–6]. Since it is not a polar crystal, for Si the piezoelectric phonon contribution should be negligibly small [10], so the relaxation is expected to be dominated by the deformation potential of acoustic phonons. The relaxation rate depends on the phonon density of states at the Zeeman energy, the amplitude of the electric fields generated by the phonons, and the strength of the SOC. The fingerprint of the deformation potential is that T_1^{-1} is expected to depend on the seventh power of the magnetic field in the limit that the wavelength of the phonon is larger than the size of the QD [1,10].

If we fit data preferentially to B^7, a proportionality constant of 0.017 (T^7 s) can be extracted. Since there is no theory that works out specifically for electron spins near the Si/SiO$_2$ interface, where the SOC is known to be dominated by the Rashba effect due to the strong electric field, we cannot further discuss this constant quantitatively. The B dependence appears to be stronger than that observed in GaAs [1] and in InGaAs [3] QDs. The data also clearly show a tendency for weaker B dependence as $B \to 0$. This residual relaxation could be caused by electrical noise generated by background charge fluctuations, as the noise can dominate when contributions from phonons rapidly diminish as $B \to 0$. Meanwhile, we cannot rule out the possibility of a different spin relaxation mechanism, which becomes more prominent as $B \to 0$. We also do not know what influence the presence of the Si/SiO$_2$ interface has on spin relaxation. Further theoretical study is well deserved.

In contrast to the $N = 1$ case, the relaxation time measured is roughly independent of the magnetic field around 5 ms for $N = 2$. Since the valley energy splitting in Si is generally unknown for QD structures [13], we do not know the exact excited states spectra to positively identify the origin of the relaxation transition, even for a two-electron QD. Normally, for a QD with paired spins, the spin relaxation involves a transition between one of the triplet states and a singlet state [1]. The relaxation rate in this case should be proportional to the phonon density of states at the transition energy. If we use the B-independent level spacing of 0.4 meV to roughly estimate the spin flipping energy, it is equivalent to a Zeeman energy at 3 T not too far off from the observed crossover of $B = 4$ T.

It should also be noted that during the preparation of this manuscript, we have received a preprint from HRL Laboratories, LLC that reported a measurement of spin relaxation time of Si/SiGe quantum dots [16]. Empirically, our T_1 of 40 ms at $B = 2$ T appears to be roughly the same as that of the Si/SiGe QD, which is shorter by a factor of 2 than that in a GaAs QD [4]. A more informative comparison, however, should be made for identical Zeeman energies and QD level spacing in order to reveal the spin-orbital coupling strength of different systems.

We have measured the spin relaxation times of a few-electron Si/SiO$_2$ based QD and studied their magnetic field dependence by an electrical pump-and-probe. Given the prominent importance of Si/SiO$_2$ based materials in mainstream electronics, it is crucial to determine whether the Si/SiO$_2$ QD is indeed a good candidate for quantum information processing. Further interesting experiments will be measurements of the phase coherence time T_2, which will tell if the promise of long phase coherence time for bulk Si can be kept in the presence of a Si/SiO$_2$ interface.

*mingx@physics.ucla.edu
[1] R. Hanson *et al.*, Rev. Mod. Phys. **79**, 1217 (2007).
[2] J. M. Elzerman *et al.*, Nature (London) **430**, 431 (2004).
[3] D. Heiss *et al.*, Solid State Commun. **135**, 591 (2005).
[4] S. Amasha *et al.*, Phys. Rev. Lett. **100**, 046803 (2008).
[5] S. Sasaki *et al.*, Phys. Rev. Lett. **95**, 056803 (2005).
[6] J. R. Petta *et al.*, Phys. Rev. B **72**, 161301(R) (2005).
[7] T. Meunier *et al.*, Phys. Rev. Lett. **98**, 126601 (2007).
[8] A. V. Khaetskii *et al.*, Phys. Rev. B **64**, 125316 (2001).
[9] V. N. Golovach *et al.*, Phys. Rev. Lett. **93**, 016601 (2004).
[10] C. Tahan *et al.*, Phys. Rev. B **66**, 035314 (2002).
[11] C. Tahan *et al.*, Phys. Rev. B **71**, 075315 (2005).
[12] D. V. Bulaev *et al.*, Phys. Rev. B **71**, 205324 (2005).
[13] S. Goswami *et al.*, Nature Phys. **3**, 41 (2007).
[14] G. M. Jones *et al.*, Appl. Phys. Lett. **89**, 073106 (2006); A. Gunther *et al.*, Superlattices Microstruct. **27**, 373 (2000); E. P. Nordberg *et al.*, Phys. Rev. B **80**, 115331 (2009).
[15] J. M. Elzerman *et al.*, Appl. Phys. Lett. **84**, 4617 (2004).
[16] R. R. Hayes *et al.*, arXiv:0908.0173.